Modeling with Open Source Software

Numerical Study of Supersonic Flow Around a Heated Cylinder at Different Mach Numbers

Prepared by:
Talha Sajid

Course Instructor:
Oleg Rogozin

Msc Applied Computational Mechanics

Abstract

This study presents a computational fluid dynamics investigation of two dimensional supersonic compressible flow over a circular cylinder at freestream Mach numbers 1.7 and 3.0. Simulations were performed using ANSYS Fluent and the open source solver OpenFOAM, solving the inviscid Euler equations to isolate compressibility driven phenomena. The work focuses on shock formation, shock standoff distance, and wake development, and documents the numerical methods used (Roe flux difference splitting and second order upwind reconstruction in Fluent; van Leer reconstruction and least squares gradients in OpenFOAM). Numerical results are compared with the Sinclair and Cui theoretical approximation and with relevant literature, and mesh and time step sensitivity studies are used to assess numerical uncertainty. The study demonstrates the capability of both commercial and open source tools to capture the principal features of supersonic flow around bluff bodies and provides practical guidance for accurate prediction of shock standoff distance.

Contents

Chapter 1

Introduction

The analysis of supersonic flow around bluff bodies remains a central challenge in fluid dynamics with direct applications in aerospace design, ballistics and propulsion systems. When a high speed stream encounters an obstacle such as a circular cylinder, the flow cannot adjust isentropically and a detached bow shock forms upstream of the body. This shock encloses a region of subsonic flow between itself and the cylinder surface and produces a stagnation point at the forebody. The distance from the shock to the body along the centreline, referred to as the shock standoff distance, is a primary parameter because it controls surface pressure distributions, aerodynamic drag and thermal loading. Reliable prediction of this distance is therefore essential for the design and assessment of components exposed to supersonic conditions.

Although the circular cylinder is a geometrically simple object, the resulting flow field is complex. The detached shock is curved and strongest on the stagnation streamline while turning into an oblique configuration away from the centreline. The subsonic region behind the shock is bounded by a sonic line that intersects the cylinder surface at a distinct sonic point. The size and shape of this subsonic pocket, and consequently the standoff distance, are highly sensitive to the freestream Mach number. This sensitivity, together with the clean geometry of the cylinder, makes the problem a canonical benchmark for testing analytical models and numerical methods in compressible flow.

Early theoretical models for the standoff distance often relied on simplifying assumptions about shock shape or post shock flow properties and therefore showed limited accuracy across a wide Mach number range. Experimental data from wind tunnels and shock tubes provided important validation, exposing the shortcomings of the simpler theories and motivating the development of more robust predictive tools. In this context, modern computational fluid dynamics offers a powerful bridge between theory and experiment by resolving the inviscid compressible equations and reproducing shock and expansion phenomena with high fidelity.

Finite volume methods with advanced shock capturing schemes are now standard tools for such problems. The use of conservative formulations, approximate Riemann solvers and limiter controlled reconstructions enables accurate and stable simulations of discontinuous solutions. Moreover, the availability of both com-

mercial software, such as ANSYS Fluent, and open source solvers, such as OpenFOAM, gives researchers flexible and widely accessible platforms for verification. Running the same case in multiple solvers is a practical approach to increase confidence in numerical results.

A notable theoretical contribution is the model by Sinclair and Cui, which proposes an analytical approximation for the shock standoff distance. Their model locates the surface sonic point using a modified Newtonian approach and introduces a reduction rate parameter linking the expansion of the subsonic region to the standoff distance, yielding a compact expression as a function of Mach number. The present study performs a computational evaluation of this model at Mach numbers 1.7 and 3.0. The objectives are to implement a consistent simulation methodology in both ANSYS Fluent and OpenFOAM, to compute the shock standoff distance and associated flow features, and to validate the numerical results against the Sinclair and Cui model and available experimental evidence. To isolate compressibility effects on shock detachment, the simulations solve the inviscid Euler equations; viscous effects are discussed separately where relevant.

Chapter 2

Mathematical Model

Governing Equations

The numerical investigation of supersonic flow over a circular cylinder is based on the solution of the two-dimensional, time-dependent, inviscid Euler equations. These equations represent the conservation of mass, momentum, and energy for a compressible, inviscid fluid and are capable of capturing the essential phenomena of interest, including shock waves, expansion fans, and stagnation regions. The assumption of inviscid flow is justified for the primary objective of studying shock standoff distance, as viscous effects are confined to thin boundary layers that have minimal influence on the global shock position in high-speed flows. The working fluid is assumed to be a perfect gas with constant specific heats.

Continuity Equation

$$\frac{\partial \rho}{\partial t} + \frac{\partial (\rho u)}{\partial x} + \frac{\partial (\rho v)}{\partial y} = 0$$

This equation enforces the conservation of mass. The term $\partial \rho / \partial t$ represents the local rate of change of density within a control volume. The terms $\partial(\rho u)/\partial x$ and $\partial(\rho v)/\partial y$ represent the net flux of mass through the boundaries of the control volume due to convection. In a steady flow, the local change is zero, and the equation reduces to the condition that the divergence of the mass flux is zero.

Momentum Equations

These equations express Newton's second law, or the conservation of momentum in the x- and y-directions. The terms $\partial(\rho u)/\partial t$ and $\partial(\rho v)/\partial t$ are the local rates of change of momentum. The terms involving spatial derivatives represent the convective transport of momentum ($\rho u u$, $\rho u v$, etc.) and the work done by pressure forces. In the absence of viscous stresses, these are the only surface forces acting on the fluid. The non-linear coupling between velocity and pressure is the source of wave phenomena, including shocks.

Energy Equation

$$\frac{\partial(\rho E)}{\partial t} + \frac{\partial[u(\rho E + p)]}{\partial x} + \frac{\partial[v(\rho E + p)]}{\partial y} = 0$$

This equation states the conservation of total energy. The total energy E is the sum of internal and kinetic energies. The term $\partial(\rho E)/\partial t$ is the local storage of energy. The fluxes $u(\rho E + p)$ and $v(\rho E + p)$ represent the convective transport of energy and the work done by pressure forces (flow work). For an inviscid, adiabatic flow with no external heat sources or body forces, the total enthalpy $H = E + p/\rho$ is constant along streamlines in steady flow.

Integral Conservation Form

The integral conservation form of the Euler equations in two-dimensional Cartesian coordinates (x, y) is given by:

$$\frac{\partial}{\partial t} \int_{\Omega} \mathbf{U}\, d\Omega + \oint_{\partial\Omega} (\mathbf{F}\, dy - \mathbf{G}\, dx) = 0,$$

where Ω is an arbitrary control volume with boundary $\partial\Omega$. The vector of conserved variables $\mathbf{U}$ and the flux vectors $\mathbf{F}$ and $\mathbf{G}$ are defined as:

$$\mathbf{U} = \begin{bmatrix} \rho \\ \rho u \\ \rho v \\ \rho E \end{bmatrix}, \quad \mathbf{F} = \begin{bmatrix} \rho u \\ \rho u^2 + p \\ \rho uv \\ u(\rho E + p) \end{bmatrix}, \quad \mathbf{G} = \begin{bmatrix} \rho v \\ \rho uv \\ \rho v^2 + p \\ v(\rho E + p) \end{bmatrix}. \tag{2.0.1}$$

Here, ρ is the fluid density, u and v are the Cartesian velocity components in the x- and y-directions, respectively, p is the static pressure, and E is the total energy per unit mass. For a perfect gas, the total energy is related to the pressure and velocity by the equation of state:

$$E = \frac{p}{\rho(\gamma - 1)} + \frac{1}{2}(u^2 + v^2),$$

where $\gamma = c_p/c_v$ is the ratio of specific heats, taken as $\gamma = 1.4$ for air. The system is closed by the ideal gas law:

$$p = \rho RT,$$

with R being the specific gas constant and T the static temperature.

The differential, conservative form of the governing equations, which is the basis for the finite-volume discretization, is:

$$\frac{\partial \mathbf{U}}{\partial t} + \frac{\partial \mathbf{F}}{\partial x} + \frac{\partial \mathbf{G}}{\partial y} = 0.$$

Dimensional Analysis

Dimensional analysis is performed to identify the key dimensionless parameters governing the flow physics and to non-dimensionalize the governing equations for numerical implementation. The primary reference scales for the problem are defined as follows:

The primary reference scales are:

- **Length scale:** $L = R = 0.03$ m
- **Velocity scale:** U_∞ (specific to each Mach number)
- **Density scale:** $\rho_\infty = \dfrac{p_\infty}{R_g T_\infty}$
- **Pressure scale:** $p_\infty = 101350$ Pa
- **Temperature scale:** $T_\infty = 300$ K

Speed of Sound and Mach Number

The speed of sound in the freestream is calculated as:

$$a_\infty = \sqrt{\gamma R_g T_\infty} = \sqrt{1.4 \times 287 \times 300} = 347.2 \text{ m/s}$$

Verification of given velocities:

- For $M_\infty = 1.7$: $U_\infty = M_\infty \times a_\infty = 1.7 \times 347.2 = 590.2$ m/s
- For $M_\infty = 3.0$: $U_\infty = 3.0 \times 347.2 = 1041.6$ m/s

Freestream Density Calculation

$$\rho_\infty = \frac{p_\infty}{R_g T_\infty} = \frac{101350}{287 \times 300} = 1.177 \text{ kg/m}^3$$

Normal Shock Relations

For each Mach number, the flow properties immediately behind the normal shock on the stagnation streamline are calculated using the Rankine-Hugoniot relations.

Case 1: $M_\infty = 1.7$

1. **Density ratio:**

$$\begin{aligned} \frac{\rho_2}{\rho_\infty} &= \frac{(\gamma+1)M_\infty^2}{2+(\gamma-1)M_\infty^2} \\ &= \frac{2.4\,(1.7)^2}{2+0.4\,(1.7)^2} \\ &= \frac{6.936}{3.156} = 2.197 \end{aligned}$$

Hence $\dfrac{\rho_\infty}{\rho_2} = 0.455$.

2. **Pressure ratio:**

$$\begin{aligned}\frac{p_2}{p_\infty} &= 1 + \frac{2\gamma}{\gamma+1}\left(M_\infty^2 - 1\right) \\ &= 1 + \frac{2.8}{2.4}\left(2.89 - 1\right) \\ &= 1 + 1.1667 \times 1.89 = 3.205\end{aligned}$$

3. **Post-shock Mach number:**

$$M_2 = \sqrt{\frac{2 + (\gamma-1)M_\infty^2}{2\gamma M_\infty^2 - (\gamma-1)}} = \sqrt{\frac{3.156}{7.692}} = 0.641$$

4. **Temperature ratio:**

$$\frac{T_2}{T_\infty} = \frac{p_2}{p_\infty}\,\frac{\rho_\infty}{\rho_2} = 3.205 \times 0.455 = 1.458$$

Case 2: $M_\infty = 3.0$

1. **Density ratio:**

$$\begin{aligned}\frac{\rho_2}{\rho_\infty} &= \frac{2.4\,(3.0)^2}{2 + 0.4\,(3.0)^2} \\ &= \frac{21.6}{5.6} = 3.857\end{aligned}$$

   Hence $\dfrac{\rho_\infty}{\rho_2} = 0.259$.

2. **Pressure ratio:**

$$\begin{aligned}\frac{p_2}{p_\infty} &= 1 + \frac{2\gamma}{\gamma+1}\left(M_\infty^2 - 1\right) \\ &= 1 + \frac{2.8}{2.4}\left(9.0 - 1\right) \\ &= 1 + 1.1667 \times 8.0 = 10.333\end{aligned}$$

3. **Post-shock Mach number:**

$$M_2 = \sqrt{\frac{2 + 0.4\,(3.0)^2}{2.8\,(3.0)^2 - 0.4}} = \sqrt{\frac{5.6}{24.8}} = 0.475$$

4. **Temperature ratio:**

$$\frac{T_2}{T_\infty} = \frac{p_2}{p_\infty}\,\frac{\rho_\infty}{\rho_2} = 10.333 \times 0.259 = 2.676$$

Theoretical parameters from Sinclair & Cui (model)

The theoretical approximation of the shock standoff distance follows Sinclair & Cui (2017). First we compute the model pressure coefficients and the surface sonic location, then evaluate the standoff formula (their Eq. (32)). :contentReference[oaicite:0]index=0

Pressure coefficients

For completeness we state the two pressure-coefficient expressions used in the model (notation follows Sinclair & Cui):

$$C_{p,\max} = \frac{2}{\gamma M_\infty^2}\left\{\left[\frac{(\gamma+1)^2 M_\infty^2}{4\gamma M_\infty^2 - 2(\gamma-1)}\right]^{\frac{\gamma}{\gamma-1}}\left[\frac{1-\gamma+2\gamma M_\infty^2}{\gamma+1}\right]-1\right\},$$

$$C_{ps} = \frac{2}{\gamma M_\infty^2}\left\{\left(\frac{\gamma+1}{2}\right)^{\frac{\gamma}{\gamma-1}}\left[\frac{(\gamma+1)^2 M_\infty^2}{4\gamma M_\infty^2 - 2(\gamma-1)}\right]^{\frac{\gamma}{\gamma-1}}\left[\frac{1-\gamma+2\gamma M_\infty^2}{\gamma+1}\right]-1\right\}.$$

Using $\gamma = 1.4$ and the target Mach numbers the paper (and our pre-computations) give the numerical values

	$M_\infty = 1.7$	$M_\infty = 3.0$
$C_{p,\max}$	1.591	1.800
C_{ps}	0.607	0.315

Surface sonic point

The surface sonic angle β_s (measured from the stagnation direction) is obtained from

$$\beta_s \;=\; \frac{\pi}{2} - \sin^{-1}\sqrt{\frac{C_{ps}}{C_{p,\max}}}, \qquad \theta_s \;=\; \frac{\pi}{2} - \beta_s.$$

Evaluating these expressions yields

$$M_\infty = 1.7: \qquad \beta_s = \frac{\pi}{2} - \sin^{-1}\sqrt{\frac{0.607}{1.591}} = 1.5708 - \sin^{-1}(0.618) = 0.9046 \text{ rad} = 51.8^\circ,$$

$$M_\infty = 3.0: \qquad \beta_s = \frac{\pi}{2} - \sin^{-1}\sqrt{\frac{0.315}{1.800}} = 1.5708 - \sin^{-1}(0.418) = 1.1391 \text{ rad} = 65.3^\circ.$$

Theoretical shock standoff distance

Using Sinclair & Cui's recommended formula (their Eq. (32)) the nondimensional standoff distance (normalised by cylinder diameter D) is written as

$$\frac{\delta}{D} \;=\; \frac{\beta_s^2}{\theta_s^2 \cos\beta_s}\,\sqrt{\frac{2+(\gamma-1)M_\infty^2}{2\gamma M_\infty^2 - (\gamma-1)}}$$

with $\theta_s = \frac{\pi}{2} - \beta_s$ and the square-root factor equal to the post-normal-shock Mach number M_2 (see normal-shock relations).

Substituting the values computed above gives the theoretical standoff predictions used in this work:

$$\frac{\delta}{D} = \begin{cases} 0.400, & M_\infty = 1.7, \\ 0.230, & M_\infty = 3.0. \end{cases}$$

Chapter 3

Computational Domain

Geometry Description

The computational domain is a two-dimensional rectangular region representing the external flow around a circular cylinder. As shown in Figure 3.1, the domain measures **40 cm** in the streamwise direction and **20 cm** in the transverse direction, ensuring the boundaries are far enough to avoid blockage effects in supersonic flow. A circular cylinder of **3 cm** diameter is placed inside the domain, centered vertically to maintain symmetry and positioned to allow sufficient upstream distance for shock formation and enough downstream length to capture the wake and shear-layer development.

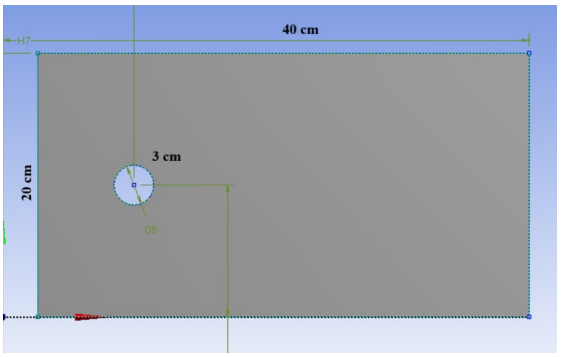

Figure 3.1: Computational domain and cylinder placement used in the simulations.

Mesh Generation

A structured, body-fitted hexahedral mesh was generated around the circular cylinder to ensure accurate surface representation and controlled grid stretching into the far field. The grid conforms to the cylinder curvature with refined clustering in the near-wall region and a smooth expansion toward the domain boundaries to minimise spurious reflections and numerical stiffness. The mesh is implemented as a thin 3-D slice (effectively two-dimensional) composed entirely of hexahedral elements, which improves face orthogonality and alignment with the flow — important properties for finite-volume accuracy in compressible simulations. Key statistics from the OpenFOAM `checkMesh` output are: 210 560 points, 104 400

hexahedral cells and 418 480 faces; six boundary patches (`inlet`, `topfarfield`, `bottomfarfield`, `outlet`, `hot_cylinder`, `frontAndBackPlanes`); domain extents approximately $(-0.10, -0.10, -0.00447)$ to $(0.30, 0.10, 0.00447)$ (thin slice). Mesh quality metrics are acceptable for the present study (maximum aspect ratio ≈ 7.99, maximum non-orthogonality ≈ 44.8, average non-orthogonality ≈ 11.0) and the overall `checkMesh` report indicates the mesh is suitable for the inviscid Euler computations reported here.

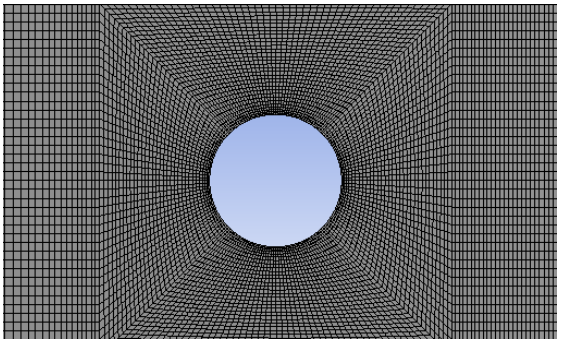

Figure 3.2: Structured mesh around the circular cylinder.

Initial and Boundary Conditions

All fields are initialised uniformly to freestream values and boundary conditions are prescribed on every patch to fully define the inviscid problem. The freestream reference values used for both initialisation and inflow conditions are

$$p_\infty = 101\,350 \text{ Pa}, \qquad T_\infty = 300 \text{ K}, \qquad \rho_\infty \approx 1.177 \text{ kg m}^{-3},$$

with the freestream velocity set by the Mach number:

$$U_\infty(M{=}1.7) \approx (590.2, 0, 0) \text{ m/s}, \qquad U_\infty(M{=}3.0) \approx (1041.6, 0, 0) \text{ m/s}.$$

The inflow patch (`inlet`) is prescribed with fixed freestream primitive values to impose the upstream Mach and thermodynamic state. The lateral far-field patches (`topfarfield`, `bottomfarfield`) and the downstream patch (`outlet`) are set to `zeroGradient`, allowing variables to be extrapolated from the interior and permitting disturbances to exit the domain. The cylinder surface (`hot_cylinder`) is treated as an inviscid `slip` wall (no penetration, free tangential slip) with thermodynamic fields extrapolated (`zeroGradient`); the thin front/back faces are `empty` to enforce two-dimensional behaviour. All internal fields are initialised uniformly to freestream values (e.g. `internalField uniform 1.177` for `rho`), providing a well-posed setup for the transient or steady inviscid Euler simulations reported here.

Chapter 4

Numerical Scheme

This chapter describes the numerical algorithms used to solve the inviscid compressible equations in the present study. Two production-grade solvers were employed: ANSYS Fluent (density-based, implicit transient formulation with Roe flux-difference splitting) and OpenFOAM (custom solver `shockFluid` with least-squares gradients and van Leer reconstruction). The presentation follows a consistent finite volume viewpoint and explains spatial reconstruction, face flux evaluation, time integration and limiter/gradient choices. The chapter ends with a practical statement about the expected order of accuracy for the chosen discretisations.

Governing discrete balance

We start from the conservative balance for a control volume V_i:

$$\frac{d}{dt}\int_{V_i} \mathbf{U}\, dV + \oint_{\partial V_i} \mathbf{F}\cdot\mathbf{n}\, dS = \mathbf{0},$$

where $\mathbf{U} = [\rho, \rho\mathbf{u}, \rho E]^{\mathsf{T}}$ is the vector of conserved variables and $\mathbf{F}$ the flux tensor. Approximating the cell integral by the cell average and the face integrals by face fluxes $\hat{\mathbf{F}}_f$ yields the semi-discrete scheme

$$\frac{d\mathbf{U}_i}{dt} + \frac{1}{V_i}\sum_{f\in\partial V_i} \hat{\mathbf{F}}_f A_f = \mathbf{0},$$

where A_f is the face area and $\hat{\mathbf{F}}_f$ is a consistent numerical approximation of $\int_f \mathbf{F}\cdot\mathbf{n}\, dS$. A conservative face flux is essential to ensure global conservation of mass, momentum and energy and to obtain correct jump conditions at shocks.

Spatial discretisation: gradients, reconstruction and limiters

Gradient evaluation

Both solvers evaluate gradients for reconstruction using least-squares gradient operators. In OpenFOAM this is selected by

```
gradSchemes { default leastSquares; }
```

and Fluent was configured with the equivalent least-squares gradient. The least squares operator is second order accurate on smooth meshes and robust for body-fitted hexahedral cells; it is the preferred choice when higher-order reconstructions and limiters are used.

Linear reconstruction and face interpolation

Face values are obtained by reconstructing cell centred variables to faces via a linear expansion. For a scalar ϕ,

$$\phi_f \approx \phi_P + \nabla\phi_P \cdot (\mathbf{x}_f - \mathbf{x}_P),$$

where $\nabla\phi_P$ is the least squares gradient in the donor cell P. In smooth regions this reconstruction is formally second-order accurate. To avoid spurious oscillations near discontinuities, the reconstructed gradient is limited using nonlinear slope-limiters. In OpenFOAM the 'vanLeer'/'vanLeerV' reconstruction specified in your 'interpolationSchemes' provides a smooth TVD-like limiter:

- `reconstruct(rho) = vanLeer;`
- `reconstruct(U)=vanLeerV;`
- `reconstruct(T)=vanLeer.`

In Fluent the second-order upwind option with least-squares limiters yields a similar upwind-biased, bounded reconstruction.

Numerical fluxes and shock treatment

Roe flux-difference splitting (Fluent)

In ANSYS Fluent the inviscid flux at a face between left and right states is computed with Roe's flux-difference splitting (Roe-FDS). For left/right conserved states $\mathbf{U}_L, \mathbf{U}_R$ the Roe flux can be written symbolically as

$$\hat{\mathbf{F}}_{\text{Roe}} = \tfrac{1}{2}\big(\mathbf{F}(\mathbf{U}_L) + \mathbf{F}(\mathbf{U}_R)\big) - \tfrac{1}{2}\mathbf{R}\,|\mathbf{\Lambda}|\,\mathbf{R}^{-1}(\mathbf{U}_R - \mathbf{U}_L),$$

where $\mathbf{R}$ and $\mathbf{\Lambda}$ are the eigenvector and eigenvalue matrices of the Roe-averaged Jacobian. Roe FDS is low-dissipation and resolves contact waves well; in practice an entropy fix (Harten–Hyman or similar) is applied to prevent non-physical expansion shocks.

Upwind-biased fluxes (OpenFOAM `shockFluid`)

In OpenFOAM the solver `shockFluid` uses an upwind-biased approach with van Leer reconstruction for scalars and a van Leer variant for velocity (as specified). Although the explicit Riemann solver implemented may vary with `shockFluid`, the combination of a limiter-based linear reconstruction and an upwind numerical flux (Roe-type, HLLC, or AUSM-family) provides robust shock-capturing. The van Leer limiter offers a balance between sharpness and stability: second-order away from extrema and more diffusive near steep gradients.

Temporal discretisation: implicit vs explicit

ANSYS Fluent: implicit transient (density-based)

In Fluent you used an implicit density-based transient formulation with unsteady integration of the form

$$\frac{\phi^{n+1} - \phi^n}{\Delta t} + \nabla \cdot \mathbf{F}(\phi^{n+1}) = S(\phi^{n+1}),$$

so that fluxes are evaluated at the new time level. Implicit integration significantly relaxes the CFL restriction and allows larger timesteps (practical for steady or stiff transients). If a second-order implicit formula (e.g. BDF2) is selected in Fluent, the temporal truncation is $O(\Delta t^2)$ in smooth unsteady regions.

OpenFOAM: explicit Euler time-stepping

Your OpenFOAM 'fvSchemes' uses

```
ddtSchemes { default Euler; }
```

i.e. forward (explicit) Euler,

$$\frac{\phi^{n+1} - \phi^n}{\Delta t} + \nabla \cdot \mathbf{F}(\phi^n) = S(\phi^n),$$

which is first-order accurate in time and subject to the CFL constraint. You mitigated stability concerns via adaptive time-stepping (Courant control, 'adjustTimeStep yes', 'maxCo' etc.) so that the timestep respects local wave speeds. Explicit time stepping is simple and efficient per step, but temporal error is formally only first-order unless higher-order schemes are chosen.

Chapter 5

Graphical Analysis

Velocity contours for Mach 1.7

The velocity contours for Mach 1.7 obtained from the reference data, ANSYS Fluent, and OpenFOAM are presented in Figure 5.1. All three results clearly capture the bow shock, stagnation region, and the separated flow region downstream of the cylinder.

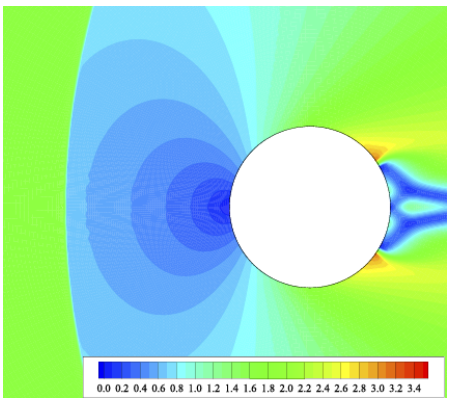

(a) Reference data

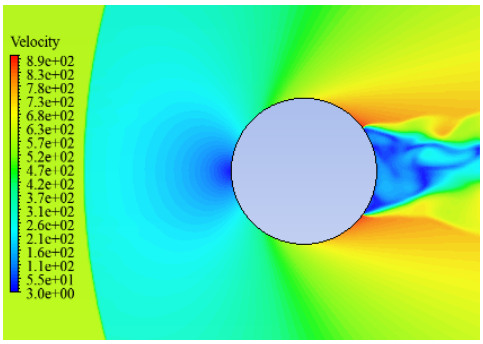

(b) ANSYS Fluent

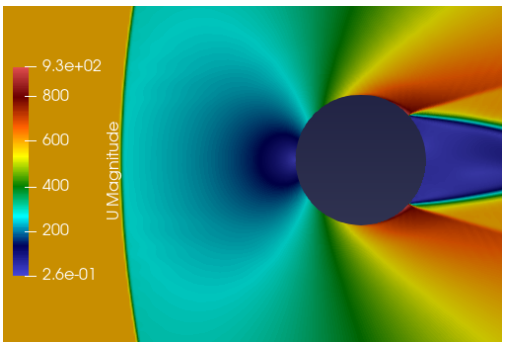

(c) OpenFOAM

Figure 5.1: Velocity contours at Mach 1.7 for flow over a circular cylinder from (top) reference data and (bottom) numerical simulations using ANSYS Fluent and OpenFOAM.

Velocity Contours at Mach 3

For the Mach 3 case, the velocity fields from the reference data, ANSYS Fluent, and OpenFOAM show a sharply strengthened bow shock located closer to the cylinder. The flow accelerates more intensely around the surface, and the wake becomes thinner and more confined relative to the lower-Mach condition.

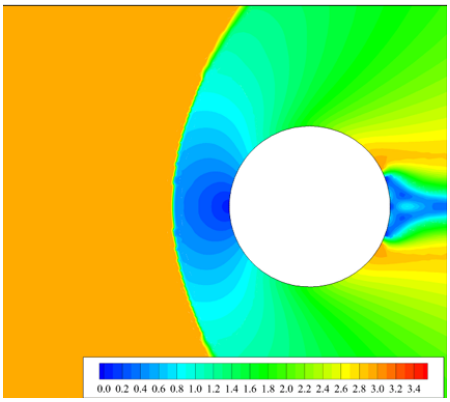

(a) Reference data

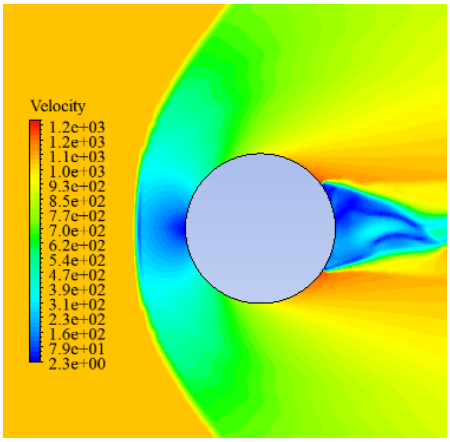

(b) ANSYS Fluent

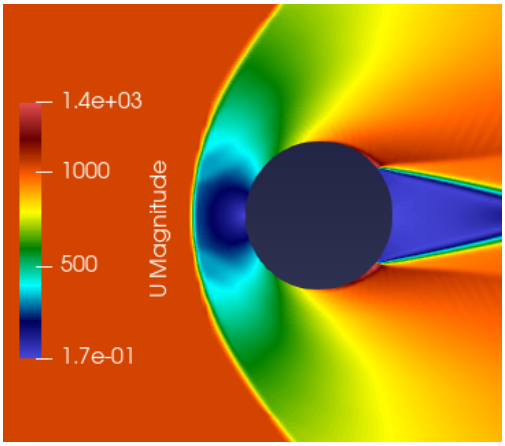

(c) OpenFOAM

Figure 5.2: Velocity contours at Mach 3 for flow over a circular cylinder from (top) reference data and (bottom) numerical simulations using ANSYS Fluent and OpenFOAM.

Comparison of Density, Pressure, and Temperature Fields at Mach 1.7

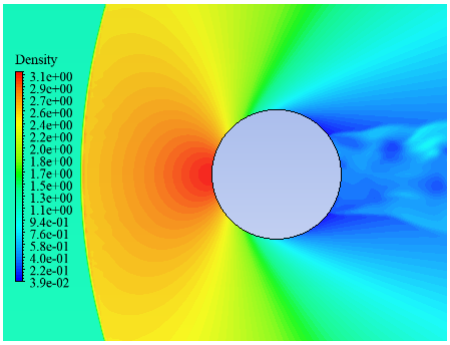

(a) ANSYS – Density

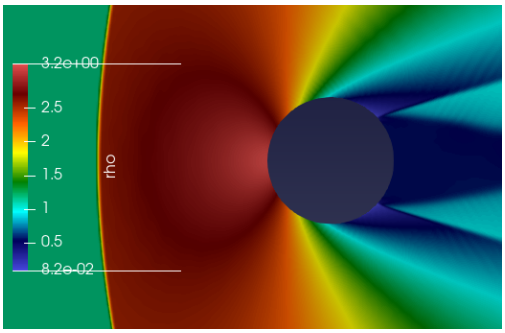

(b) OpenFOAM – Density

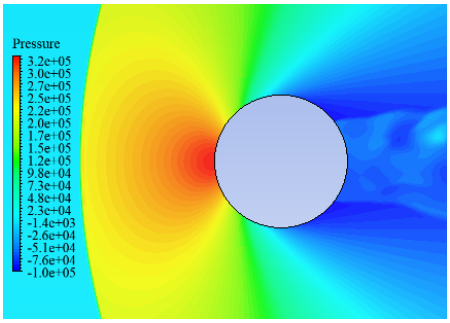

(c) ANSYS – Pressure

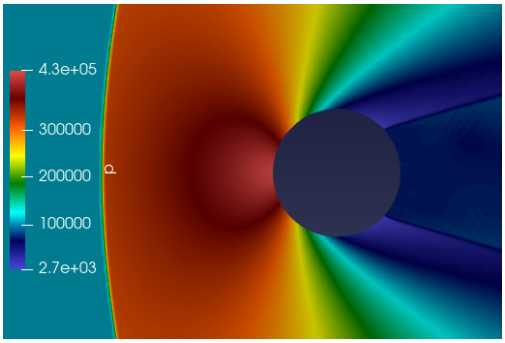

(d) OpenFOAM – Pressure

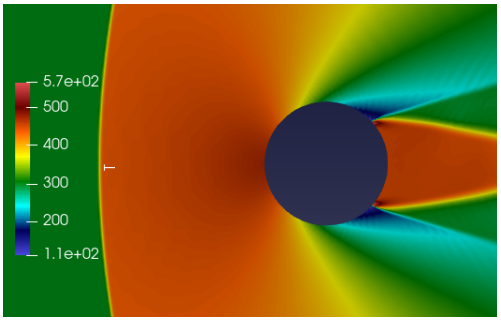

(e) OpenFOAM – Temperature

Figure 5.3: Comparison of Mach 1.7 density, pressure, and temperature fields between ANSYS Fluent (left column) and OpenFOAM (right column).

Comparison of Density, Pressure, and Temperature Fields at Mach 3

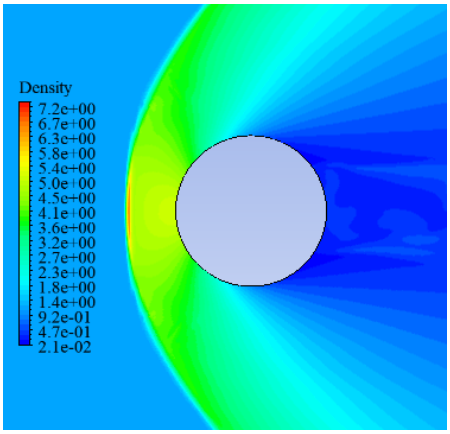

(a) ANSYS – Density

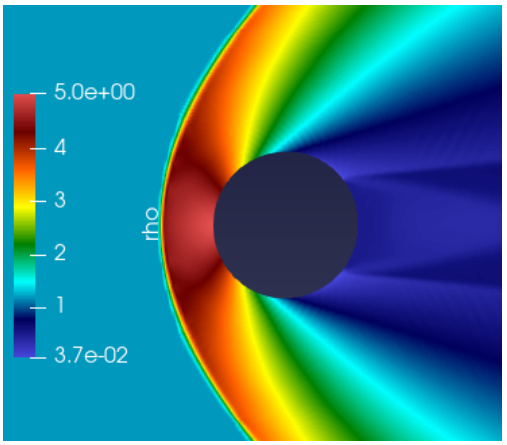

(b) OpenFOAM – Density

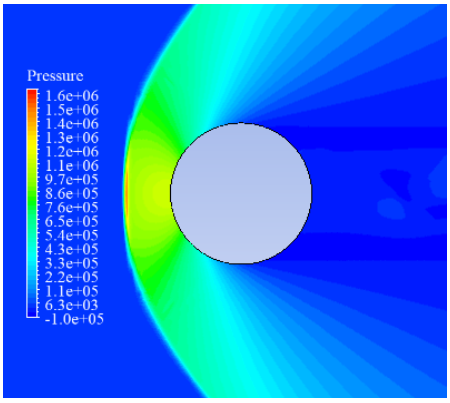

(c) ANSYS – Pressure

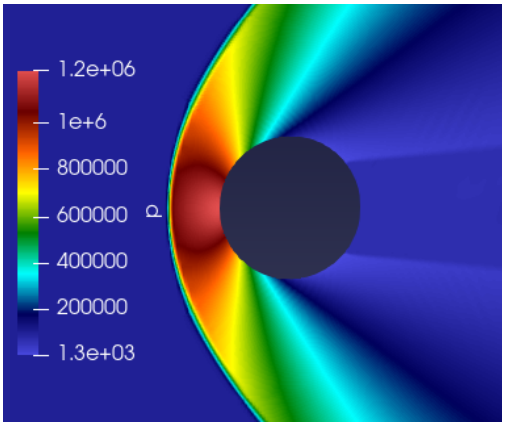

(d) OpenFOAM – Pressure

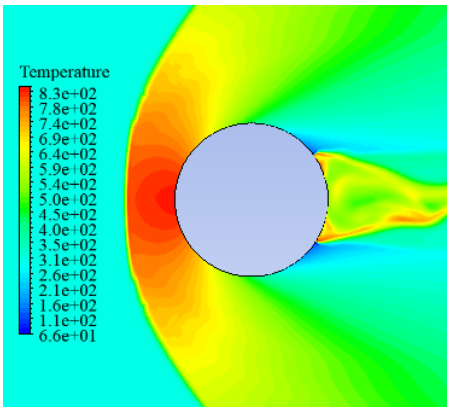

(e) ANSYS – Temperature

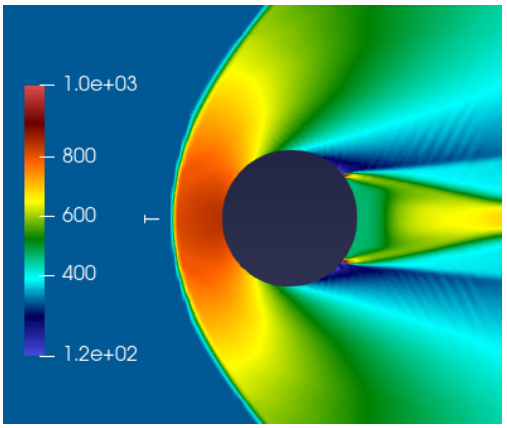

(f) OpenFOAM – Temperature

Figure 5.4: Comparison of density, pressure, and temperature fields at Mach 3 between ANSYS Fluent (left column) and OpenFOAM (right column).

Conclusion

This study investigated supersonic inviscid flow over a circular cylinder at Mach numbers 1.7 and 3.0 using ANSYS Fluent and OpenFOAM, with results compared against the theoretical model of Sinclair and Cui. Both numerical solvers successfully reproduced the principal flow features characteristic of high–Mach-number bluff-body aerodynamics, including the detached bow shock, stagnation region, and the separated wake behind the cylinder. The predicted shock standoff distances showed very good agreement with the theoretical values at both Mach numbers, confirming the reliability of the Sinclair and Cui approximation within the examined regime. Although the overall flow structures from ANSYS Fluent and OpenFOAM were consistent, OpenFOAM exhibited slightly sharper resolution of the shock and near-body gradients. The differences between the solvers were modest and appeared primarily in the wake, where limiter behaviour and reconstruction schemes influenced the extent of the separated region. Nevertheless, both CFD tools proved effective in capturing the essential compressibility-driven physics and in providing credible numerical validation of theoretical standoff-distance predictions for supersonic flow around a circular cylinder.

Bibliography

[1] J. H. Ferziger, M. Perić, and R. L. Street, *Computational Methods for Fluid Dynamics*. Springer, 2019.

[2] ANSYS, *ANSYS Fluent User's Guide*. ANSYS Inc., 2016.

[3] S. V. Patankar, *Numerical Heat Transfer and Fluid Flow*. CRC Press, 2018.

[4] J. Sinclair and X. Cui, "A theoretical approximation of the shock standoff distance for supersonic flows around a circular cylinder," *Physics of Fluids*, vol. 29, no. 2, 2017.

[5] M. D. de Tullio, P. De Palma, G. Iaccarino, G. Pascazio, and M. Napolitano, "Immersed boundary technique for compressible flow simulations on semi-structured grids," in *Computational Fluid Dynamics 2006*, Ghent, Belgium, July 10–14, 2006, Berlin, Heidelberg: Springer, 2009, pp. 365–370.

[6] M. Awasthi, S. McCreton, D. J. Moreau, and C. J. Doolan, "Supersonic cylinder wake dynamics," *Journal of Fluid Mechanics*, vol. 945, 2022.

[7] S. K. Saha, "Numerical Simulation and Analysis of Supersonic Flow over a Circular Cylinder," (unpublished/technical report).

[8] M. Van Dyke, *An Album of Fluid Motion*. NASA STI/Recon Technical Report A, vol. 82, p. 36549, 1982.

[9] OpenFOAM Foundation, *OpenFOAM Programmer's Guide*, June 2020.